CrossMark

ARTICLE

Monotonic and cyclic mechanical reliability of metallization lines on polymer substrates

Oleksandr Glushko
Erich Schmid Institute of Materials Science, Austrian Academy of Sciences and Department of Material Physics, Montanuniversität Leoben, Leoben A-8700, Austria

Andreas Klug[b)]
NanoTecCenter Weiz Forschungsgesellschaft mbH, Weiz A-8160, Austria

Emil J.W. List-Kratochvil
Institut für Physik, Institut für Chemie & IRIS Adlershof, Humboldt-Universität zu Berlin, Berlin 12489, Germany

Megan J. Cordill[a)]
Erich Schmid Institute of Materials Science, Austrian Academy of Sciences and Department of Material Physics, Montanuniversität Leoben, Leoben A-8700, Austria

(Received 30 January 2017; accepted 20 March 2017)

Mechanical stability of Ag and Cu printed and evaporated metallization lines on polymer substrates is investigated by means of monotonic tensile and cyclic bending tests. It is shown that lines which demonstrate good performance during monotonic tests fail at lower strains during a cyclic bending tests. Evaporated lines with the grain size of several hundreds of nanometers have good ductility and consequently good stability during monotonic loading but at the same time they fail at low strains during cyclic bending. Printed lines with nanocrystalline microstructure, in contrast, demonstrate more intensive cracking during monotonic loading but higher failure strains during cyclic bending. Apart from the grain size effect, the effect of film thickness on the saturation crack density after cyclic bending is also demonstrated. Thinner films have higher crack density in accordance with the shear lag model.

I. INTRODUCTION

Electronics developed for flexible applications, such as rollable displays, wearable sensors, circuitry or flexible batteries,[1–5] need to have the ability to stretch and bend without failure. This attribute is in contrast to rigid electronic counterparts which mostly fail through electrical degradation or thermal-mechanical instabilities, such as electromigration, crack formation, or interface delamination. Much research has gone into determining failure mechanisms and fatigue lifetimes of materials used in flexible electronics. Methods include *in situ* tensile straining to study crack and deformation evolution,[6–8] stress–strain development with X-ray diffraction (XRD),[8–11] and interface adhesion measurements.[12–14] The electrical behavior can also be examined with tensile straining with two- or four-point-probe resistance geometry incorporated into the grips[15–17] or with wires attached to the sample[18,19] for tensile straining. The advantage of *in situ* resistance measurements is the precise measurement of the crack onset strain (COS), or failure strain, of brittle films and lines, such as transparent conductive oxides or brittle metals. The COS can be considered the threshold for stretching of flexible technologies. Not only the COS of brittle materials can be determined with *in situ* resistance measurements during straining, but also the electrical degradation with continued strain and any resistance recovery during the unloading of the strain.[16,20] Both the COS and electrical degradation can be used to evaluate the influence of thickness, microstructure, and deposition method.

Bending techniques have also been developed to address the rollable and bending applications and are necessary to prove flexibility.[21–26] The use of bending tests also better simulates real-life loading conditions. The bending tests provide information about the strain below which no damage or fracture occurs and when performed cyclically, a lifetime curve can be determined by the number of cycles the system can withstand at a given strain before damage is observed. Bending strain at which failure occurs is important for flex-to-connect applications where the device is only bent once, while cyclic bending is necessary for rollable or foldable applications when many bending cycles are expected.

Contributing Editor: Erik G. Herbert
[a)]Address all correspondence to this author.
e-mail: megan.cordill@oeaw.ac.at
[b)]Present Address: AVL List GmbH, Hans-List-Platz 1, A-8020 Graz, Austria, andreas.klug@avl.com
DOI: 10.1557/jmr.2017.121

 © Materials Research Society 2017

https://doi.org/10.1557/jmr.2017.121 Published online by Cambridge University Press

The development of reliability curves from bending tests provide important information about the lifetime of metal and ceramic films on flexible substrates.[22] However, different research groups have different definitions of the number of cycles to failure for films on substrates depending on the detection method used. When resistance is the detection parameter, then the number of cycles to failure is determined when the relative resistance increases 2%[26] or even 20–25%.[25,27] Other definitions of the number of cycles to failure include when the extrusion density reaches saturation[28–30] or simply using the first cycle where damage is observed.[31]

Many studies have addressed the role of film thickness,[25,32,33] the annealing treatments of printed Ag films,[26,34–36] and the fabrication method (printing versus evaporation),[26,34] however, the combined role of film thickness and film microstructure has not been thoroughly addressed for monotonic and cyclic bending tests. In this paper, Ag and Cu metallization lines with different thicknesses and microstructures are characterized by means of monotonic tensile straining and cyclic bending tests in combination with *in situ* resistance measurements and post-mortem electron microscopy. It is shown that high ductility crucial for good reliability during a monotonic tensile test may act as a drawback limiting the mechanical stability under cyclic loading. Further examination of the mechanical behavior demonstrates that the grain size and film thickness are the main length scale parameters which strongly influence the mechanical performance of conductive lines.

II. MATERIALS AND METHODS

An overview of six different sample types, namely evaporated and printed silver as well as evaporated copper lines, considered in this paper are listed in Table I. All lines have the width of 0.5 mm and the length of 40 mm. The evaporated silver lines were produced in a vacuum coating unit using a base pressure less than 1×10^{-6} mbar and a deposition rate of 10 Å/s. Three different nominal thicknesses were deposited, 100, 400, and 800 nm on 130 μm thick PEN (polyethylene naphthalene, Teonex® Q65HA, Teijin DuPont Films, Tokyo, Japan) substrates using a silver source (purity 99.95%) without additional substrate heating. For comparison, Cu lines with the thickness of 800 nm were also evaporated onto 180 μm thick PET (polyethylene terephthalate, Melinex® ST506, Teijin DuPont Films) substrates using the same vacuum coating unit and shadow mask. For the inkjet printed lines, a PiXDRO LP50 printer equipped with FujiFilm Dimatix Spectra S-Class SE-128 piezoelectric print head (FujiFilm, Tokyo, Japan) was utilized with silver ink CCI-300 from Cabot Corporation (Boston, Massachusetts). During printing the substrate temperature was kept constant at 60 °C to obtain a print resolution of 800 dpi. Samples were sintered at 150 °C for 2 h in a drying oven after printing. The printed lines were fabricated on the same PEN and PET substrates as the evaporated lines and have a nominal thickness of 800 nm. Initial resistances of all lines measured using the distance between the contacts of 39 mm are given in Table I. Since all lines have the same width one can conclude that the resistivity of the printed lines is about an order of magnitude higher than the resistivity of evaporated lines which is common for printed Ag.[26,34] The grain sizes of evaporated lines were determined using electron-backscatter diffraction mapping (EBSD). The particle size of the printed lines were taken from the ink specifications and confirmed by direct scanning electron microscopy (SEM) imaging to be between 30 and 80 nm.

In situ tensile straining with four-point-probe resistance measurements were performed on an MTS Tyron 250® Universal testing machine (MTS Systems, Eden Prairie, Minnesota) using a constant displacement rate of 5 μm/s for loading to 20% strain and unloading to zero force. For each material system, at least four tests were performed with the probing contacts incorporated into the grips and measured with a Keithley 2000 multimeter (Keithley Instruments, Cleveland, Ohio) as described in more detail in Refs. 15 and 16. After straining, samples were examined with SEM and the average saturation crack densities after 20% strain were determined with a linear line intercept method.

The bending tests were performed using a newly developed apparatus called FLEX-E-TEST.[22] The samples are clamped at one end in grips which are fixed to a motor-driven wheel. Each grip has a curvature radius corresponding to the required bending radius to be applied during the test. During rotation the samples sequentially come into contact with the bending surface and bend to the corresponding grip radius (Fig. 1). Three different bending radii of 5, 10, and 20 mm were used in bending experiments.

TABLE I. Summary of samples and initial characteristics.

Sample name	Substrate & thickness (μm)	Method & metal	Thickness (nm)	Initial resistance (Ohm)	Grain or particle size (nm)
eTeAg100	PEN (Teonex), 130	Evap. Ag	100	25	100–250
eTeAg400	PEN (Teonex), 130	Evap. Ag	400	5	400–600
eTeAg800	PEN (Teonex), 130	Evap. Ag	800	2.2	500–800
pTeAg800	PEN (Teonex), 130	Printed Ag	700–800	25	30–80
pMeAg800	PET (Melinex), 180	Printed Ag	700–800	35	30–80
eMeCu800	PET (Melinex), 180	evap. Cu	800	2.2	700–900

https://doi.org/10.1557/jmr.2017.121 Published online by Cambridge University Press

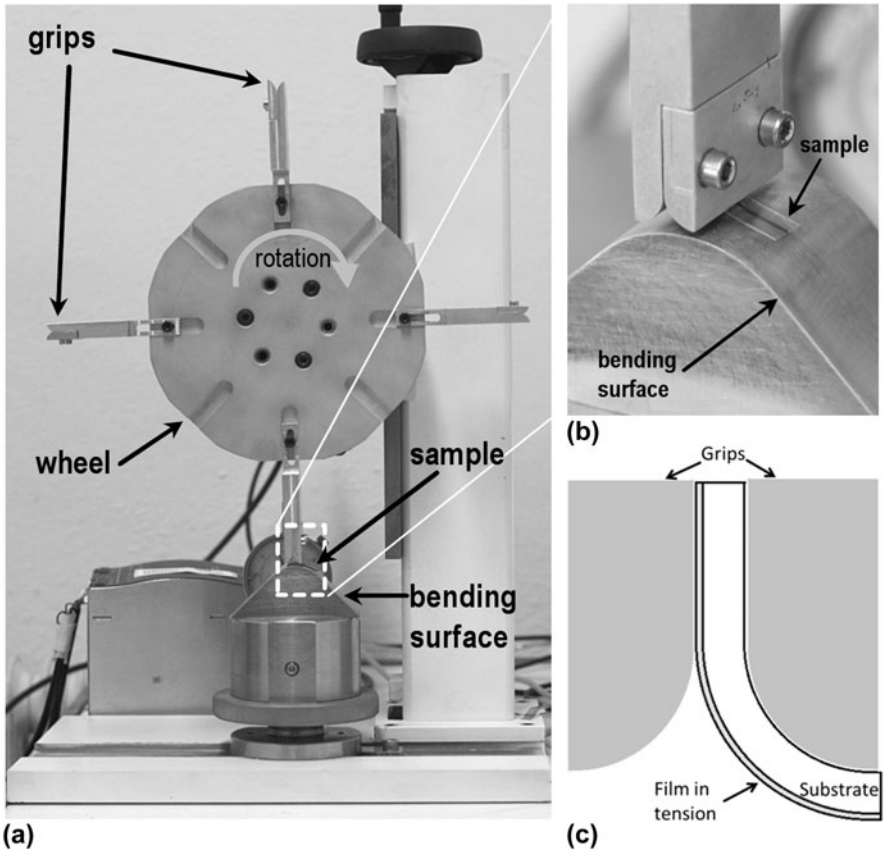


FIG. 1. Photograph of the of FLEX-E-TEST bending wheel (a). The sample is clamped between curved grips with a defined radius so that when the sample comes into contact with the bending surface, a defined bending strain is applied (b). When the film is on the outside of the grip, a tensile bending strain is applied (c).

The bending strain, ε, was estimated using the general formula $\varepsilon = d_s/2r$, where d_s is the substrate thickness and r is the bending radius of the grip. Note that the PET substrates are slightly thicker than the PEN substrates (Table I) which results in higher strains under the same bending radius. To analyze the evolution of the damage in the lines a series of tests were performed with different numbers of bending cycles between 100 and 5×10^4. For each maximum cycle number three different samples were tested to exclude the effects of possible fabrication defects. The amount of mechanical damage induced by cyclic bending was characterized in terms of the linear crack density. The crack density was calculated by taking a series of SEM micrographs after a given number of bending cycles. For each micrograph the number of cracks per unit length was determined and then averaged.

III. RESULTS

A. Monotonic tensile straining

An overview of the behavior of the electrical resistance during monotonic tensile straining to a maximum strain of 20% is shown in Fig. 2(a) for the evaporated lines and in Fig. 2(b) for printed lines. Each curve has a loading portion which starts at zero strain, increasing to the maximum strain of 20% and an unloading portion, as shown by the arrows in Fig. 2. Following the common and well-justified practice,[15,37] the constant volume approximation ($R/R_o = (L/L_o)^2$, where R is the measured resistance, R_o is the initial resistance, L is the measured gauge length and L_o is the initial gauge length), which shows the resistance behavior in the case of perfect plastic deformation without cracking (dashed "theory" curve), was used as a reference curve. The point where the experimentally measured relative resistance (R/R_o) starts to deviate from the constant volume approximation curve defines the value of the COS. The 400 and 800 nm thick evaporated silver lines as well as the 800 nm thick evaporated copper lines demonstrate very good mechanical stability [Fig. 2(a)] because the resistance follows the constant value approximation curve up to the strain of approximately 12%. Furthermore, at the maximum strain of 20% the deviation from the theoretical curve is moderate compared to the 100 nm thick evaporated silver lines. Such resistance behavior suggests that the applied strain induced only short, isolated cracks or localized deformation. The resistance of the 100 nm thick evaporated silver line starts to deviate from the theoretical

https://doi.org/10.1557/jmr.2017.121 Published online by Cambridge University Press

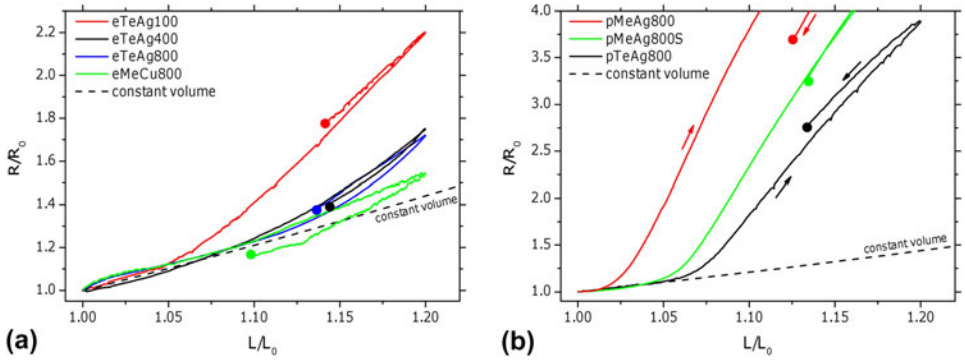


FIG. 2. Representative relative electrical resistance measured *in situ* during straining as a function of the relative gauge length for evaporated lines (a) and printed lines (b). The arrows indicate the loading and unloading portions. Solid circles depict the values of resistance and strain at zero force. The dashed theory line represents the constant volume approximation.

curve after only 5% strain and reaches a higher value at the maximum strain (120% resistance increase). Faster growth of resistance with decreasing film thickness was previously observed[25,37] and is explained by the lower ductility of the thinner films, most likely due to the smaller grain size.

The resistance of the printed silver lines grows by several hundred percent as the strain is increased to 20% [Fig. 2(b)]. Such a strong deviation from the theoretical curve indicates that extensive cracking occurred during straining. Indeed, since the size of silver particles used for printing lie well below 100 nm, plastic deformation through dislocation slip[38] is prohibited, resulting in rather brittle behavior. The values of COS for the printed lines are in the range of 5%. It is necessary to note, that for many flexible electronics applications which do not involve elastomeric substrates, there is no need to prove high stability at such high strains as 20%. Much more important is good reliability at low strains below 3%. This consideration is based on the fact that polymer substrates such as PEN, PET, and polyimide start to deform plastically for strains above 3% and should not be used in device applications requiring higher strains. Thus, for this lower strain regime printed Ag lines on PEN and PET show very good stability comparable to that of evaporated Ag lines.

Another important aspect of the *in situ* resistance experiments is that all of the relative resistance curves shown in Fig. 2 demonstrate resistance recovery during unloading. The solid circles depict the resistance of fully unloaded samples when the applied load has reached zero. As it was shown in Ref. 16 this resistance recovery is caused by both the mechanical relaxation of the substrate and crack closure. The thicker Ag and Cu evaporated lines almost completely recover indicating extensive crack re-bridging. This behavior is often overlooked but is highly important to accurately predict the real electrical behavior.

The differences in the *in situ* resistance behavior discussed above are also manifested in the morphology of the mechanical damage induced in the lines during tensile straining. Figure 3 presents a comparison of the damage of three evaporated silver lines of different thickness, the printed Ag lines on PEN and PET, as well as the evaporated Cu line is presented. Note that all micrographs are at the same magnification. The 100 nm thick evaporated Ag lines [Fig. 3(a)] exhibit clear channel cracks with lengths up to several micrometers and an average crack density of $0.33 \pm 0.03\ \mu m^{-1}$ after 20% strain [Fig. 3(a)]. This observation explains the faster growth of the electrical resistance of 100 nm thick evaporated lines [Fig. 2(a)]. The evaporated 400 and 800 nm thick Ag lines exhibit very short cracks and locally thinned areas indicating that plastic deformation occurred during straining [Figs. 3(b)–3(c)]. Since concurrent plastic deformation and cracking occurred, an accurate crack density is difficult to determine with SEM micrographs. However, if only channel cracks are considered for the 400 nm evaporated film, then the average crack density was determined to be $0.13 \pm 0.02\ \mu m^{-1}$ after 20% strain. The decrease of the saturation crack density with increasing films thickness is expected when comparing the same material and deposition method. The printed Ag lines on PEN and PET [Figs. 3(d)–3(e)] have clear channel cracks, some of which have re-connected due to the removal of the applied load. After 20% strain printed lines revealed an average crack density of $0.22 \pm 0.04\ \mu m^{-1}$ on PEN and $0.12 \pm 0.03\ \mu m^{-1}$ on PET. The difference is most likely due to the nominal thickness variation of the substrate or is an indication of the interface shear strength. The 800 nm evaporated Cu lines reveal no cracking but areas of localized deformation [Fig. 3(f)].

B. Cyclic bending reliability

For applications of repeated bending the recently developed FLEX-E-TEST technique[22] was used. The damage induced in the conductive lines was characterized

https://doi.org/10.1557/jmr.2017.121 Published online by Cambridge University Press

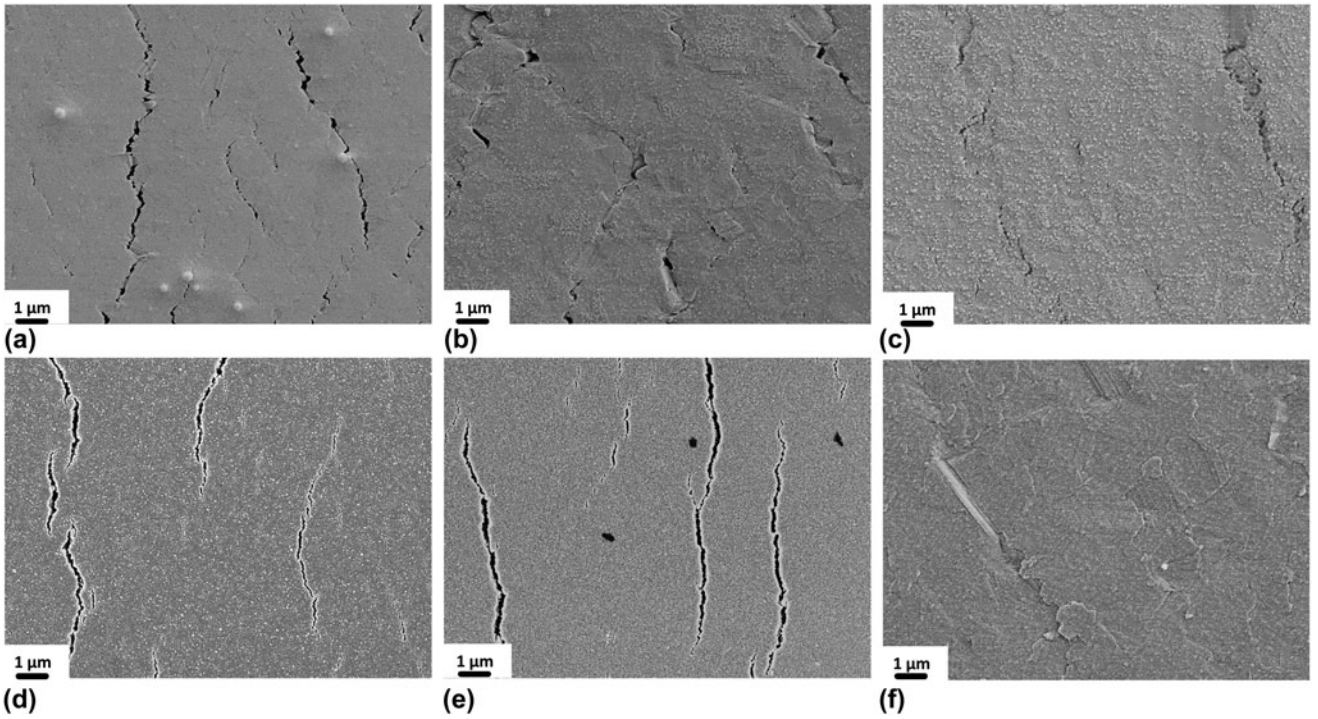


FIG. 3. Typical post-mortem SEM micrographs showing the surface of (a) 100 nm thick evaporated Ag, (b) 400 nm thick evaporated Ag, (c) 800 nm thick evaporated Ag, (d) 800 nm thick printed Ag on PEN, (e) 800 nm printed Ag on PET, and (f) 800 nm evaporated Cu after monotonic tensile straining to 20%.

by the linear crack density. For simplicity and clarity only the effect of tensile bending cycles will be considered below. The comparison of tensile, compressive, and mixed bending is given in detail elsewhere.[22]

The dependence of the crack density on the cycle number for the evaporated silver lines with three different thicknesses is shown in Figs. 4(a) and 4(b) for 5 and 10 mm bending radii, respectively. In the case of the 5 mm bending radius (1.3% strain), the crack density saturates after a few hundred cycles (approx. 500) for all three thicknesses. The crack density, however, depends strongly on the film thickness, with the largest values found for 100 nm thick lines and the lowest for 800 nm thick lines. In the case of the 10 mm bending radius (0.65% strain), the crack density of the 100 nm thick lines does not start to increase until after 1×10^4 cycles and has the lowest value compared to the 400 and 800 nm thick lines after 5×10^4 cycles. Due to the small grain size (100–250 nm) the dislocation-based slip mechanisms are restricted in the 100 nm thick lines and the applied strain of 0.65% is too low to induce intensive homogeneous cracking. A similar behavior was observed in 200 nm evaporated Cu films subjected to 1.1% bending strain.[25] In contrast, dislocations in the 400 and 800 nm thick lines can move at very small strains and accumulate damage quickly with the cycle number because of the larger grain size and increased thickness.

The SEM micrographs of evaporated and printed lines after 5×10^4 cycles with 1.3% bending strain are shown in Fig. 5. All micrographs are taken at the same magnification. The effect of film thickness is clearly manifested in Figs. 5(a)–5(c) where the 100 nm thick lines demonstrate long channel cracks running parallel to each other. Such fracture morphology is typical for rather brittle films although localized plastic deformation in the form of surface extrusions can be seen along the cracks. The 800 nm thick evaporated Ag lines [Fig. 5(c)] exhibit significant plasticity, which is manifested by numerous slip bands and large extrusions along the cracks. Evidence of plastic deformation was not observed in the printed lines [Figs. 5(d)–5(e)] where the film surface between the cracks is not deformed by cyclic loading as observed in the evaporated lines. The 800 nm evaporated Cu lines [Fig. 5(f)] behave in a similar manner as the 800 nm evaporated Ag lines illustrating extrusions and cracks. The saturation crack densities of the 100 and 400 nm evaporated Ag films after 5×10^4 cycles of 1.3% bending strain relate well to the monotonic crack densities after 20%. At lower bending strains, however, the values strongly deviate, with the corresponding reasons still under investigation.

The concept of fatigue life, which is defined as the number of cycles to failure, is difficult to apply when characterizing the fatigue failure of polymer-supported films. The main reason is that the films do not completely

https://doi.org/10.1557/jmr.2017.121 Published online by Cambridge University Press

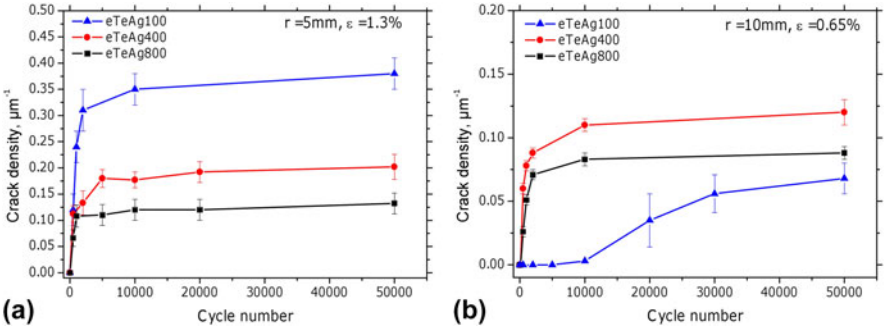


FIG. 4. The dependence of the linear crack density on the number of tensile bending cycles for evaporated lines with three different thicknesses and bending radii of (a) 5 mm and (b) 10 mm.

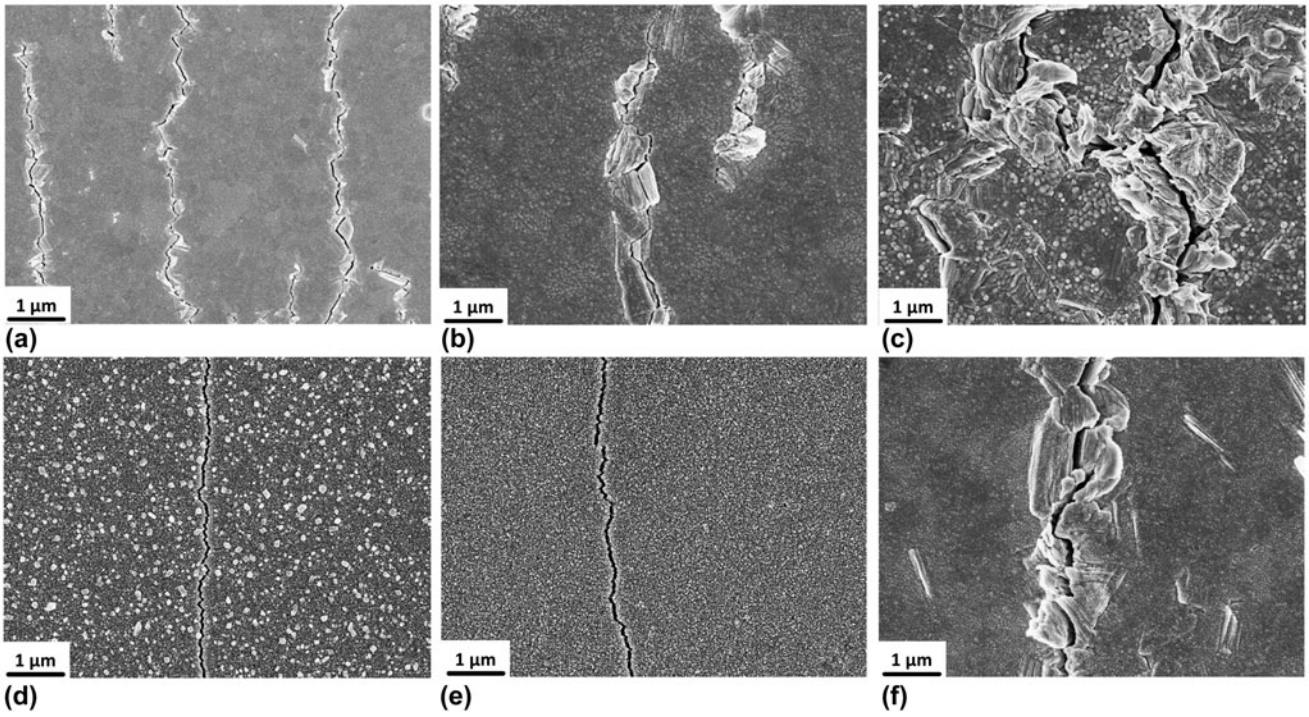


FIG. 5. Typical post-mortem SEM micrographs showing the surface of (a) 100 nm thick evaporated Ag, (b) 400 nm thick evaporated Ag, (c) 800 nm thick evaporated Ag, (d) 800 nm thick printed Ag on PEN, (e) 800 nm thick printed Ag on PET, and (f) 800 nm evaporated thick Cu on PET after 5×10^4 tensile bending cycles with a bending strain of 1.3% (a–d) and 0.9% (e and f).

fracture due to the polymer substrate. This makes a clear and universal definition of failure impossible, but, as mentioned already, several groups have attempted to define failure criteria.[26,27,31,39] Since the cyclic bending method used here does not measure resistance as a function of bending, the following failure criteria is proposed. From the point of view of flexible electronic applications one can define the minimum number of bending cycles which a device must sustain during the entire expected lifetime. Assuming that a device should be able to be bent ten times per day for the lifetime of 10 years, a critical number of 36,500 cycles is obtained. Taking into account possible defects and irregularities during the fabrication process, a more conservative value of 5×10^4 cycles seems to be adequate. The cyclic reliability of a flexible component can then be visualized by plotting the dependence of a reliability parameter, such as the electrical resistance or crack density, as a function of the applied strain or bending radius after 5×10^4 cycles. Such dependencies of the crack density after 5×10^4 cycles on the applied bending strain are shown in Fig. 6, where the different printed and evaporated lines with the same thickness of 800 nm on PET and PEN are compared. The most distinct feature of the reliability curves is the existence of a threshold strain for the printed lines below which the crack density is zero. This threshold strain is estimated to be at least 0.4% for printed lines, which is much lower than the COS

https://doi.org/10.1557/jmr.2017.121 Published online by Cambridge University Press

value (5%) obtained from monotonic tensile straining [Fig. 2(b)]. In the case of the 800 nm thick evaporated lines the crack density is non-zero even at the lowest applied strains of 0.33% for both copper and silver making the difference to the COS (12%) even more drastic. What the reliability curves also illustrate is, that despite the monotonic behavior, printed lines are better than evaporated lines at bending strains less than 0.6%. One should also notice that the evaporated Ag lines and the printed Ag on PEN have very similar crack densities at strains between 0.6 and 1.3% despite significant differences in their microstructures. This observation suggests that the saturation crack density is predominantly defined by the film thickness as is well known for monotonic testing using the shear lag theory.[40–42]

IV. DISCUSSION

The presented results illustrate that there is a significant gap between the mechanical reliability assessment obtained from monotonic tensile tests and cyclic bending tests. In the case of monotonic tensile tests the ductility of a thin film is the crucial property which determines the electro–mechanical performance. The more ductile the film, which is controlled by the resulting microstructure, the closer the electrical response is to the constant volume approximation and fewer cracks are induced during straining as demonstrated in Fig. 3. High ductility, however, acts as a drawback under cyclic loading conditions. It is known that in ductile metals dislocations can move at very low strains, typically below 0.1%. During a single bending cycle dislocations can be activated and accumulated with increasing cycles, leading to the formation of extrusions and cracks even at low cyclic strains (Fig. 5). The printed lines and, to some extent, the 100 nm thick evaporated lines have restricted ductility due to the small grain or particle size. This is clearly demonstrated by the lower COS values deduced from a monotonic tensile test (Fig. 2). At the same time, if the applied mechanical strains remain below the threshold value, then no damage is induced even after 5×10^4 bending cycles. This threshold strain corresponds to the true elastic limit stress below which the deformation is purely elastic. The exact value of the elastic strain limit is difficult to determine since it depends on the fabrication technique, thickness, and resulting microstructure, but also on the density of defects which can act as crack-initiation sites.

Apart from the grain size effect on the reliability there is a strong effect of film thickness on the saturation crack density [Fig. 4(a)]. The dependence of the saturation crack density on film thickness can be understood with the help of a shear lag model.[41–43] Formation of a crack in a thin film on a substrate results in stress relaxation in the immediate vicinity of the crack. Due to the stress relaxation the next crack can appear only at some distance away from the existing crack. This distance, which corresponds to the minimum crack spacing, was shown to depend directly on the film thickness being smaller for thinner films and larger for thicker films.[40–43]

Although the shear lag model, in general, considers intrinsically brittle films under increasing monotonic strain it can be qualitatively applied to the cracks induced by cyclic loading. The dependencies of the film stress on the distance from the crack edge calculated using the shear lag solution provided by Hsueh & Yanaka[41]

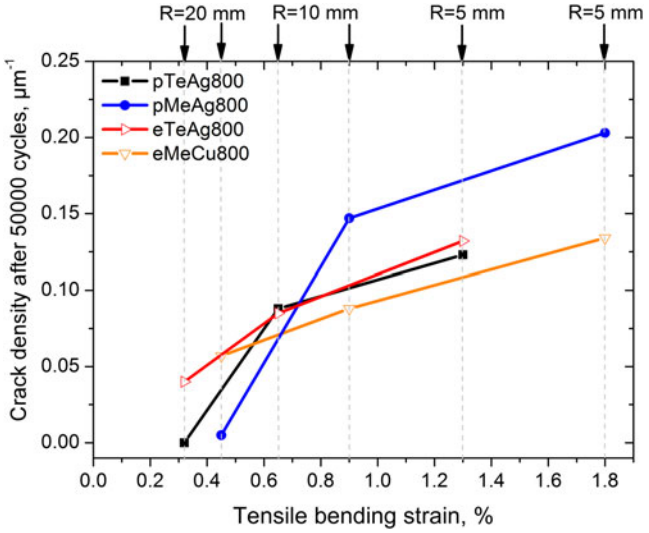


FIG. 6. Cyclic reliability curves showing the dependence of the crack density after 5×10^4 cycles on the applied bending strain. Two evaporated and two printed lines with the same thickness of 800 nm on two different substrates are shown (see also Table I).

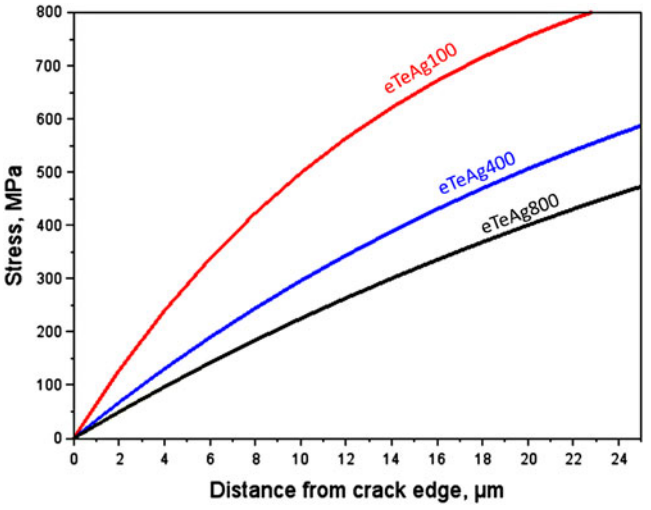


FIG. 7. Film stress versus the distance from the crack edge for three silver films with different thicknesses obtained from shear lag model solution taken from Ref. 41.

https://doi.org/10.1557/jmr.2017.121 Published online by Cambridge University Press

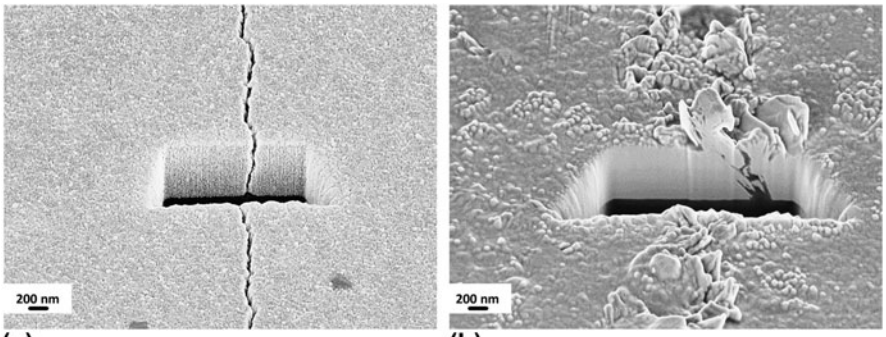


FIG. 8. Focused ion beam cross-sections of the cracks induced by cyclic bending in 800 nm printed Ag film (a) and 800 nm thick evaporated Ag film (b).

for three different thicknesses of silver films on PEN under applied strain of 1.3% are shown in Fig. 7. Assuming that the next crack can propagate if some critical stress value is reached, the 100 nm thick films will have the shortest crack-to-crack distance and the 800 nm thick film will have the larger distance between cracks, as observed in Fig. 4(a). The exact determination of this critical stress cannot be accomplished using shear lag model since it is a one-dimensional model and the stress concentration at the tip of a propagating crack is not considered.

Although the saturation crack density is predominantly defined by a films thickness, the crack morphology is still dependent on the film microstructure and grain size. The focused ion beam cross-sections of the 800 nm thick printed film and the evaporated film with the same thickness are shown in Fig. 8. It is clearly seen that the printed film exhibits a brittle crack running perpendicularly to the surface without local thinning or significant plastic deformation. The evaporated film shows the extrusion-crack couple with the voids at the interface indicating that accumulation of dislocation based slip is responsible for the crack formation.

As a final remark one should notice that the evaporated copper films demonstrate electrical and deformation behavior similar to evaporated silver of the same thickness and grain size which confirms that these two length scale effects play a dominant role in the determination of mechanical reliability. This could indicate that the material (i.e., Cu or Ag) used is secondary to the microstructure and thickness in terms of reliability.

V. SUMMARY

It was shown that different mechanisms are behind the electro–mechanical reliability determined by monotonic tensile and cyclic bending tests. In the case of monotonic tensile straining, the COS is predominantly determined by the ductility of the film which, depends more on the grain size. The fact that 400 nm thick evaporated silver lines, 800 nm thick evaporated silver lines, and 800 nm thick evaporated copper lines all have similar COS values and similar grain sizes of several hundred nanometers supports this finding. The nanocrystalline printed lines demonstrate low COS and significant cracking at 20% strain resulting in low crack densities. The 100 nm thick evaporated Ag lines represent an intermediate case showing relatively low COS, high crack density, but moderate resistance increase at 20% strain. Monotonic tensile straining can be used to determine how far film-substrate couples can be stretched without cracking, which provides information about the ductility of the film.

The cyclic bending reliability depends more on film thickness and the applied strain. When the applied cyclic strain is high enough for crack initiation and propagation, then the film thickness is the dominant parameter defining the resulting crack density. This explains why the crack density of the evaporated and printed films with the same thickness are very similar despite the differences in the microstructure. At low cyclic strains, however, the value of the minimum strain to activate a dislocation source comes into play. In nanocrystalline materials the dislocation motion is restricted due to the small grain or particle size. For cyclic strains of 0.4% the printed films remain purely elastic and cracks did not form after 5×10^4 cycles. In the evaporated films of the same thickness dislocation slip is activated at much lower strains and accounts for the nonzero crack density at the cyclic strain of 0.33%. Among the considered metallization lines the best combination of cyclic and monotonic reliabilities was demonstrated by the inkjet printed silver on PEN, which has a relatively high crack onset strain of 5% as well as zero crack density for cyclic strains below 0.4%.

ACKNOWLEDGMENTS

This work was partially supported by the Austrian Research Promotion Agency (FFG) through the program “Produktion der Zukunft”, Project 843648 and the Austrian Science Fund (FWF) through project P27432-N20.

https://doi.org/10.1557/jmr.2017.121 Published online by Cambridge University Press

REFERENCES

1. S. Nau, C. Wolf, S. Sax, and E.J.W. List-Kratochvil: Organic nonvolatile resistive photo-switches for flexible image detector arrays. *Adv. Mater.* **27**, 1048 (2015).
2. S. Nau, C. Wolf, K. Popovic, A. Blümel, F. Santoni, A. Gagliardi, A. di Carlo, S. Sax, and E.J.W. List-Kratochvil: Inkjet-printed resistive switching memory based on organic dielectric materials: From single elements to array technology. *Adv. Electron. Mater.* **1**, 140003-1 (2015).
3. I. Graz, M. Kaltenbrunner, C. Keplinger, R. Schwödiauer, S. Bauer, S.P. Lacour, and S. Wagner: Flexible ferroelectret field-effect transistor for large-area sensor skins and microphones. *Appl. Phys. Lett.* **89**, 073501-1 (2006).
4. M. Koo, K. Il Park, S.H. Lee, M. Suh, D.Y. Jeon, J.W. Choi, K. Kang, and K.J. Lee: Bendable inorganic thin-film battery for fully flexible electronic systems. *Nano Lett.* **12**, 4810 (2012).
5. A. Klug, P. Patter, K. Popovic, A. Blümel, S. Sax, M. Lenz, O. Glushko, M.J. Cordill, and E.J.W. List-Kratochvil: Recent progress in printed 2/3D electronic devices. In. *Proc. Spie* **9569**, E.J.W. List Kratochvil, ed. (SPIE, San Diego, 2015); p. 95690N.
6. N.C. Woo, K. Cherenack, G. Tröster, and R. Spolenak: Designing micro-patterned Ti films that survive up to 10% applied tensile strain. *Appl. Phys. A* **100**, 281 (2010).
7. N. Lu, X. Wang, Z. Suo, and J.J. Vlassak: Metal films on polymer substrates stretched beyond 50%. *Appl. Phys. Lett.* **91**, 221909-1 (2007).
8. V.M. Marx, F. Toth, A. Wiesinger, J. Berger, C. Kirchlechner, M.J. Cordill, F.D. Fischer, F.G. Rammerstorfer, and G. Dehm: The influence of a brittle Cr interlayer on the deformation behavior of thin Cu films on flexible substrates: Experiment and model. *Acta Mater.* **89**, 278 (2015).
9. S. Olliges, P.A. Gruber, V. Auzelyte, Y. Ekinci, H.H. Solak, and R. Spolenak: Tensile strength of gold nanointerconnects without the influence of strain gradients. *Acta Mater.* **55**, 5201 (2007).
10. S. Frank, U.A. Handge, S. Olliges, and R. Spolenak: The relationship between thin film fragmentation and buckle formation: Synchrotron-based in situ studies and two-dimensional stress analysis. *Acta Mater.* **57**, 1442 (2009).
11. P.A. Gruber, E. Arzt, and R. Spolenak: Brittle-to-ductile transition in ultrathin Ta/Cu film systems. *J. Mater. Res.* **24**, 1906 (2009).
12. M.J. Cordill, F.D. Fischer, F.G. Rammerstorfer, and G. Dehm: Adhesion energies of Cr thin films on polyimide determined from buckling: Experiment and model. *Acta Mater.* **58**, 5520 (2010).
13. B. Erdem Alaca, M.T.A. Saif, and H. Sehitoglu: On the interface debond at the edge of a thin film on a thick substrate. *Acta Mater.* **50**, 1197 (2002).
14. J. Andersons, S. Tarasovs, and Y. Leterrier: Evaluation of thin film adhesion to a compliant substrate by the analysis of progressive buckling in the fragmentation test. *Thin Solid Films* **517**, 2007 (2009).
15. O. Glushko and M.J. Cordill: Electrical resistance of metal films on polymer substrates. *Exp. Tech.* **40**, 303 (2016).
16. O. Glushko, V.M. Marx, C. Kirchlechner, I. Zizak, and M.J. Cordill: Recovery of electrical resistance in copper films on polyethylene terephthalate subjected to a tensile strain. *Thin Solid Films* **552**, 141 (2014).
17. A. Wyss, M. Schamel, A.S. Sologubenko, R. Denk, M. Hohage, P. Zeppenfeld, and R. Spolenak: Reflectance anisotropy spectroscopy as a tool for mechanical characterization of metallic thin films. *J. Phys. D: Appl. Phys.* **48**, 415303-1 (2015).
18. G.D. Sim, Y. Hwangbo, H.H. Kim, S.B. Lee, and J.J. Vlassak: Fatigue of polymer-supported Ag thin films. *Scr. Mater.* **66**, 915 (2012).
19. N. Lambricht, T. Pardoen, and S. Yunus: Giant stretchability of thin gold films on rough elastomeric substrates. *Acta Mater.* **61**, 540 (2013).
20. B. Putz, R.L. Schoeppner, O. Glushko, D.F. Bahr, and M.J. Cordill: Improved electro-mechanical performance of gold films on polyimide without adhesion layers. *Scr. Mater.* **102**, 23 (2015).
21. S-H. Choa, C-K. Cho, W-J. Hwang, K. Tae Eun, and H-K. Kim: Mechanical integrity of flexible InZnO/Ag/InZnO multilayer electrodes grown by continuous roll-to-roll sputtering. *Sol. Energy Mater. Sol. Cells* **95**, 3442 (2011).
22. O. Glushko, M.J. Cordill, A. Klug, and E.J.W. List-Kratochvil: The effect of bending loading conditions on the reliability of inkjet printed and evaporated silver metallization on polymer substrates. *Microelectron. Reliab.* **56**, 109 (2016).
23. Q. Guan, J. Laven, P.C.P. Bouten, and G. de With: Mechanical failure of brittle thin films on polymers during bending by two-point rotation. *Thin Solid Films* **611**, 107 (2016).
24. W.P. Vellinga, J.T.M. De Hosson, and P.C.P. Bouten: Direct measurement of intrinsic critical strain and internal strain in barrier films. *J. Appl. Phys.* **110**, 044907-1 (2011).
25. B.J. Kim, H.A.S. Shin, J.H. Lee, T.Y. Yan, T. Haas, P. Gruber, I.S. Chou, O. Kraft, and Y.C. Joo: Effect of film thickness on the stretchability and fatigue resistance of Cu films on polymer substrates. *J. Mater. Res.* **29**, 2827 (2014).
26. B-J. Kim, T. Haas, A. Friederich, J-H. Lee, D-H. Nam, J.R. Binder, W. Bauer, I-S. Choi, Y-C. Joo, P.A. Gruber, and O. Kraft: Improving mechanical fatigue resistance by optimizing the nanoporous structure of inkjet-printed Ag electrodes for flexible devices. *Nanotechnology* **25**, 125706-1 (2014).
27. G-D. Sim, Y-S. Lee, S-B. Lee, and J.J. Vlassak: Effects of stretching and cycling on the fatigue behavior of polymer-supported Ag thin films. *Mater. Sci. Eng., A* **575**, 86 (2013).
28. R. Schwaiger and O. Kraft: Size effects in the fatigue behavior of thin Ag films. *Acta Mater.* **51**, 195 (2003).
29. O. Kraft, P. Wellner, M. Hommel, R. Schwaiger, and E. Arzt: Fatigue behavior of polycrystalline thin copper films. *Zeitschrift Fuer Met. Res. Adv. Tech.* **93**, 392 (2002).
30. G.P. Zhang, C.A. Volkert, R. Schwaiger, E. Arzt, and O. Kraft: Damage behavior of 200-nm thin copper films under cyclic loading. *J. Mater. Res.* **20**, 201 (2005).
31. D. Wang, P.A. Gruber, C.A. Volkert, and O. Kraft: Influences of Ta passivation layers on the fatigue behavior of thin Cu films. *Mater. Sci. Eng., A* **610**, 33 (2014).
32. P.A. Gruber, J. Böhm, F. Onuseit, A. Wanner, R. Spolenak, and E. Arzt: Size effects on yield strength and strain hardening for ultra-thin Cu films with and without passivation: A study by synchrotron and bulge test techniques. *Acta Mater.* **56**, 2318 (2008).
33. M.J. Cordill and A.A. Taylor: Thickness effect on the fracture and delamination of titanium films. *Thin Solid Films* **589**, 209 (2015).
34. S. Kim, S. Won, G-D. Sim, I. Park, and S-B. Lee: Tensile characteristics of metal nanoparticle films on flexible polymer substrates for printed electronics applications. *Nanotechnology* **24**, 085701-1 (2013).
35. J.R. Greer and R.A. Street: Thermal cure effects on electrical performance of nanoparticle silver inks. *Acta Mater.* **55**, 6345 (2007).
36. S. Gamerith, A. Klug, H. Scheiber, U. Scherf, E. Moderegger, and E.J.W. List: Direct ink-jet printing of Ag-Cu nanoparticle and Ag-precursor based electrodes for OFET applications. *Adv. Funct. Mater.* **17**, 3111 (2007).
37. N. Lu, Z. Suo, and J.J. Vlassak: The effect of film thickness on the failure strain of polymer-supported metal films. *Acta Mater.* **58**, 1679 (2010).
38. C.S. Pande and K.P. Cooper: Nanomechanics of Hall–Petch relationship in nanocrystalline materials. *Prog. Mater. Sci.* **54**, 689 (2009).

https://doi.org/10.1557/jmr.2017.121 Published online by Cambridge University Press

39. O. Glushko, A. Klug, E.J.W. List-Kratochvil, and M.J. Cordill: Relationship between mechanical damage and electrical degradation in polymer-supported metal films subjected to cyclic loading. *Mater. Sci. Eng., A* **662**, 157 (2016).
40. D.C. Agrawal and R. Raj: Measurement of the ultimate shear strength of a metal–ceramic interface. *Acta Metall.* **37**, 1265 (1989).
41. C.H. Hsueh and M. Yanaka: Multiple film cracking in film/substrate systems with residual stresses and unidirectional loading. *J. Mater. Sci.* **38**, 1809 (2003).
42. M. Yanaka, Y. Tsukahara, N. Nasako, and N. Takeda: Cracking phenomena of brittle films in nanostructure composites analysed by a modified shear lag model with residual strain. *J. Mater. Sci.* **33**, 2111 (1998).
43. F. Ahmed, K. Bayerlein, S.M. Rosiwal, M. Göken, and K. Durst: Stress evolution and cracking of crystalline diamond thin films on ductile titanium substrate: Analysis by micro-Raman spectroscopy and analytical modelling. *Acta Mater.* **59**, 5422 (2011).

https://doi.org/10.1557/jmr.2017.121 Published online by Cambridge University Press